ISBN: 978-3-95450-219-6 ISSN: 2226-0366 doi: 10.18429/JACoW-LINAC2024-TUPB019

A NOVEL TEST CAVITY SETUP FOR SURFACE CONDUCTIVITY MEASUREMENTS OF ADDITIVE MANUFACTURING SAMPLES

M. Mayerhofer[1], G. Dollinger[1], R. Helm[1], J. Sonpar[2], H. Hähnel[2]
[1]Bundeswehr University Munich, 85579 Neubiberg, Germany
[2]Goethe University Frankfurt, 60438 Frankfurt am Main, Germany

Abstract

Additive Manufacturing (AM) has the potential to increase the performance of radio frequency (rf) cavity resonators while cutting manufacturing costs. To leverage this potential, AM processes and potentially post-processing techniques must be tailored to cavity requirements. Additionally, conventional manufacturing's quality assurance methods must adapt to the AM case requiring numerous studies on additively manufactured test bodies. We introduce a compact rf cavity design, enabling cost-effective and precise studies of the surface conductivity of test bodies. The test body is mounted on a dielectric holder inside a cylindrical rf cavity made of aluminum. The geometry of the test body corresponds to a rod which allows simple and cost-effective production, post-processing and evaluation. The test body's surface conductivity is extracted from a measurement of the quality factor (Q_0) of the cavity. Depending on the geometry of the test body, Q_0 values of over 10,000 can be achieved for copper test bodies. Thereby, the test body is responsible for up to two-thirds of the total cavity loss. Studies will be presented demonstrating the precision of surface conductivity determination via Q-measurement and the impact of uncertainties in test body position and geometry

INTRODUCTION

Conventional manufacturing of RF cavity resonators is expensive and design constraints limit performance [1,2]. Studies show that additive manufacturing (AM), especially Laser Powder Bed Fusion (L-PBF), have the potential to produce higher-performing cavities at lower costs [3–11]. For example, optimized cooling channels can improve cooling efficiency. However, after printing, AM cavities show higher surface roughness than conventionally manufactured ones, decreasing surface conductivity (σ_S). Current post-processing techniques aim to reduce this roughness to achieve desired quality factors (Q_0) [8, 11]. Nevertheless, predicting the surface roughness-σ_S relationship remains challenging, necessitating direct Q_0 measurements on whole AM cavities or cavities with AM manufactured complex internal geometries [3, 4, 8].

These geometries are time-consuming and expensive to produce. Moreover, these complex geometries make it difficult to compare different post-processing methods and to characterize the part's surface. We propose a test cavity setup for rapid, precise σ_S evaluation on simple test bodies. The symmetrical geometry of the test bodies allows uniform post-processing and straightforward roughness analysis. Hence, this setup enables an efficient comparison of post-processing methods and an optimization of the RF cavity manufacturing process without the need for complex and costly geometries. A cost-effective and uniform generation of an empirical data set can be achieved for the development of a Roughness-Q_0 methodology.

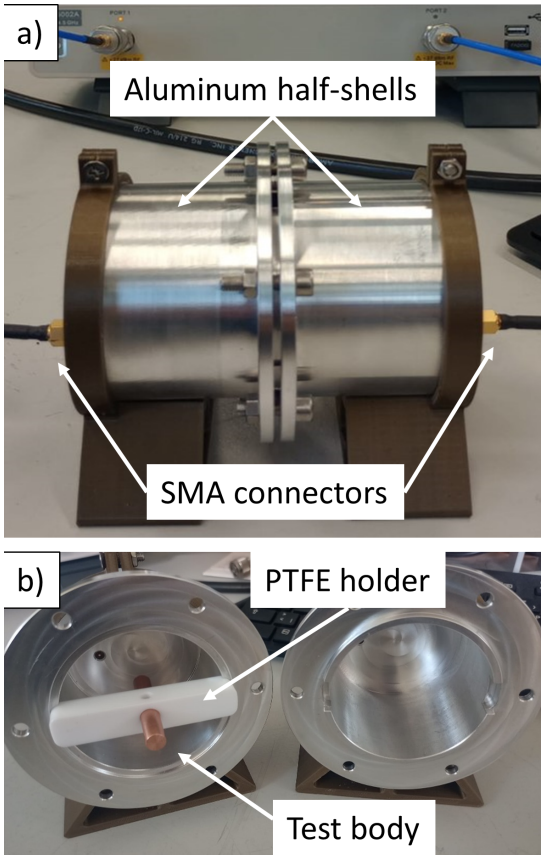

Figure 1: Test cavity a) mounted and connected to the VNA and b) in individual parts

MATERIALS AND METHODS

The test cavity setup is shown in Fig. 1a. Two bolted aluminum half-shells form the actual cavity. Each half-shell is equipped with an SMA connector for coupling of the rf signal. The disassembled test cavity is shown in Fig. 1b. The test body, mounted on a holder made of PTFE, is located in the center of the test cavity. In this study, three test bodies are examined: one made of oxygen-free copper annealed for 3 hours at 530 °C, one made of oxygen-free copper that was not annealed, and one additively manufactured from

ISBN: 978-3-95450-219-6 ISSN: 2226-0366 doi: 10.18429/JACoW-LINAC2024-TUPB019

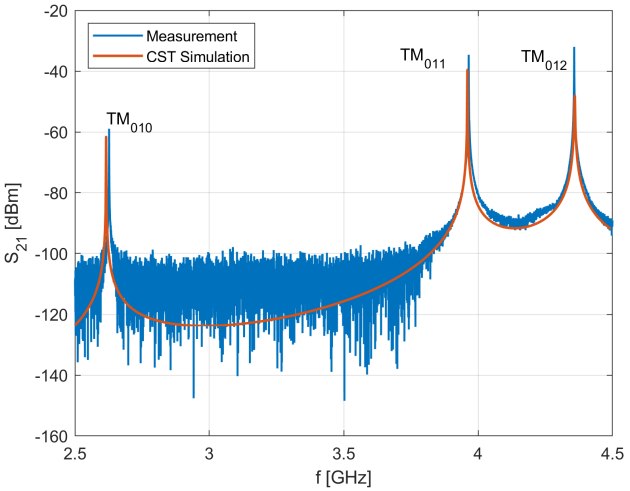

Figure 2: S_{21} simulated with CST and measured with the VNA in the range of 2.5 GHz to 4.5 GHz.

$AlSi_{10}Mg$ in the as-printed condition. Hereinafter referred to as AOFC, OFC and ASM.

Q_0 is determined using a vector network analyzer (VNA) through a S_{21} measurement under weak coupling conditions ($\beta << 1$). The simulations were conducted using the 3D EM software CST Studio Suite (CST), employing the frequency domain solver. The surface conductivity of the test body is given by

$$\sigma_S = \sqrt{\frac{\sigma}{\pi f \mu}}\,, \tag{1}$$

where f is the rf frequency, μ is the magnetic permeability, and σ is the electrical bulk conductivity of the test body (e.g., 58 MS/m for annealed copper). For $f = 2.73$ GHz as simulated for the TM_{010} mode, σ_S corresponds to approx. 2320 S. The aluminum halves were screwed together with a torque of 5 Nm for each measurement. In the longitudinal direction, the test body position was aligned using calipers.

RESULTS

Figure 2 shows the signal transmitted through the cavity from Port 1 to Port 2 (S_{21}) as a function of the excitation frequency f for the AOFC test body (σ of 58 MS/m). The VNA measurement and the CST simulation are plotted in orange and blue, respectively. The Q_0 of the TM_{010}, TM_{011} and TM_{012} mode simulated with CST are 11700, 12517, and 11302, respectively. The corresponding Q_0-values measured with the VNA are 10830 ± 30, 11200 ± 30, and 10300 ± 30. The measured Q_0 values are therefore between 7 % and 10 % lower than simulated. For the TM_{010} mode, the empty cavity (without holder and test body) shows a simulated and measured Q_0 of 14100 and 12800 ± 30, respectively. Figure 3 shows the simulated resonance curves of the cavity modes with test body in detail. In addition, the orange line shows the resonance curves for a 50 % reduced σ of 29 MS/m simulated with CST, resulting in a reduction of the Q_0 of the individual modes by 10 %, 1 %, and 2 %.

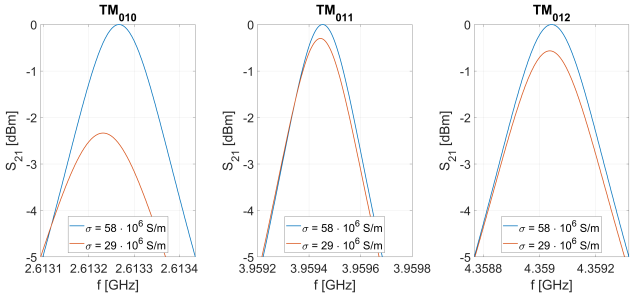

Figure 3: Resonance curves of the TM_{010}, TM_{011} and TM_{012} modes simulated with CST in detail. In blue and orange for $\sigma = 58$ MS/m and $\sigma = 29$ MS/m, respectively.

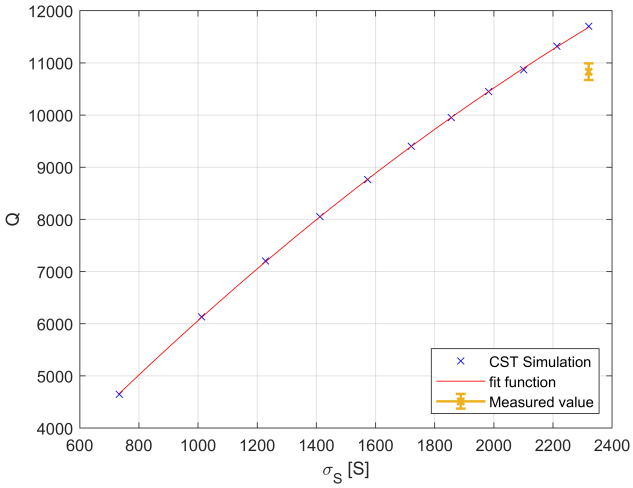

Figure 4: Q_0 of the TM_{010} mode in dependence of the test body's σ_S. Simulated values marked with blue and associated fit curve in red. In orange, the measured Q_0 for the annealed AOFC test body.

The dependence of TM_{010} mode's Q_0 on σ_S is shown in Fig. 4. The blue data points represent the relationship simulated with CST. The measured Q_0 for the TM_{010} mode with the AFCO test body is shown in orange. The fit function for the simulated values corresponds to

$$Q_0 = -0.00061246 \cdot \sigma_S^2 + 6.193 \cdot \sigma_S + 341.9\,, \tag{2}$$

and is shown in red.

Figure 5 shows how Q_0 of the TM_{010} mode responds to a deviation (Δ) of the longitudinal positioning (Δx), the diameter (Δd) or the length (Δl) of the test body, respectively. The dashed blue line represent the measurements for different longitudinal test body positions (Δx). A Δx of 1 mm reduces Q_0 by approx. 0.5 %. A Δd and Δl of 0.4 mm results in a Q_0 reduction of approx. 2.0 % and 0.8 %, respectively.

Figure 6 shows the measured S_{21} as a function of f around the TM_{010} mode for the AOFC test body, the OFC test body, and the ASM test body. The measured Q_0 values for these test bodies are 10830 ± 30, 9320 ± 30 and 6190 ± 30 respectively.

ISBN: 978-3-95450-219-6 ISSN: 2226-0366 doi: 10.18429/JACoW-LINAC2024-TUPB019

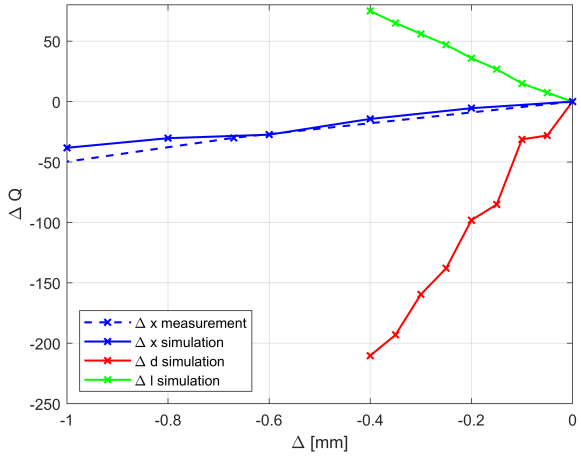

Figure 5: Impact of deviation (Δ) in longitudinal positioning (Δx), diameter (Δd) and length (Δl) of the test body on Q_0 of the TM_{010} mode.

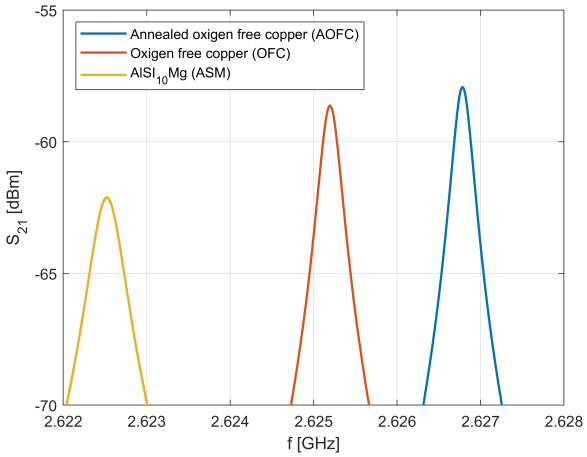

Figure 6: S_{21} measured arround the TM_{010} mode for the ASM, OFC and AOFC test body, respectively.

DISCUSSION

As seen in Fig. 3, the measured TM_{010}, TM_{011}, and TM_{012} modes are clearly identifiable and well-separated from each other. The CST simulation with reduced σ_s identifies the TM_{010} mode as most suitable for the measurements, as it's Q_0 is most sensitive to σ_s-changes.

The fit function giving the dependence of Q_0 on the surface conductivity σ_S (see Fig. 4) is used to derive the σ_S of other test bodies. However, the measured Q_0 of the TM_{010} mode is reduced by 8 % to 10 % compared to the simulated Q_0. This reduction between simulation and measurement applies as well to the empty cavity. We are therefore of the opinion that the loss in Q_0 can be attributed to the contact resistance, surface roughness and the alloy composition of the aluminum cavity halves. To derive the unknown σ_S of other test bodies, we decided to adjust the fit function to:

$$Q_0 = -0.00061246 \cdot \sigma_S^2 + 6.193 \cdot \sigma_S - 500 \,, \qquad (3)$$

which corresponds to the measured Q_0 for the TM_{010} mode for the AOFC (cf. Fig. 4) or a reduction of the ordinate intercept by approximately 7 %.

Figure 3 shows that the test body can be positioned with an accuracy of less than 0.25 mm in longitudinal direction, resulting in a relative uncertainty of at most 0.1 % in Q_0. Relative changes of the test body diameter or longitudinal dimension have a higher impact as Q_0 compared to relative changes in positioning. Therefore it is important to consider that each post-processing method results in some material removal. Previous studies indicate that up to 300 µm must be removed from AM cavities to achieve the desired Q_0 [8, 9]. This could result in a Q_0 uncertainty of approx. 3 %.

However, [7] showed that the expected material removal can be anticipated, achieving geometric accuracy of up to 10 µm, and therefore a Q_0 uncertainty of less than 0.3 %. The influence of larger geometric deviations can always be estimated by measuring the test body and subsequently adapting the fit function with CST simulated results. The error in Q_0 measurement due to the VNA is estimated to be ±30 (approx. 0.3 %). Therefore, we assume that the combined measurement uncertainty from positioning accuracy, geometric deviation and VNA is

$$\sqrt{0.1\%^2 + 0.3\%^2 + 0.3\%^2 + 0.3\%^2} \approx 0.6\% \,. \qquad (4)$$

For the two measured Q_0 values of the test bodies OFC, and ASM (see Fig. 6), the fit function and error estimation yield surface conductivities σ_S of (1969 ± 12) S, and (1230 ± 8) S, respectively. This corresponds to bulk conductivity σ of (40.18 ± 0.49) MS/m and (15.68 ± 0.20) MS/m. Since the setup was calibrated with AOFC, its σ_S matches the literature value. The reduction in σ_S of OFC compared to AOFC corresponds to approx. 15 %. The ASM shows a reduction of approx. 47 % compared to the AOFC. However, especially for AM samples, a precise analysis of the test objects is necessary for a quantitative evaluation. For example, density variations during printing can lead to a reduction in σ. The high surface roughness resulting with AM and potential chemical impurities further influence σ_S [8, 9, 12].

CONCLUSION

The presented test cavity setup allows for evaluating the surface conductivity σ_S of a test body with a measurement uncertainty of under 1 % without the need for costly and complex test cavities or other geometries. Instead, the symmetrical geometry of the test body ensures uniform post-processing and simplifies the analysis of surface roughness. Compared to other setups for similar tasks, such as $\lambda/4$ resonators [13], the test body has no electrical connection to the cavity, eliminating any measurement uncertainty that could arise from the quality of such a connection. Therefore, the test cavity setup enables an easy and qualitative comparison of different post-processing methods and the acquisition of an empirical dataset for a Roughness-Q_0 model.

ISBN: 978-3-95450-219-6 ISSN: 2226-0366 doi: 10.18429/JACoW-LINAC2024-TUPB019

REFERENCES

[1] I. H. Wilson, "Cavity construction techniques", presented at CERN Accelerator School, CERN, Geneva, Switzerland, 1992. doi:10.5170/CERN-1992-003.375

[2] A. Nassiri *et al.*, "History and technology developments of radio frequency (RF) systems for particle accelerators", *IEEE Transactions on Nuclear Science*, vol. 63, no. 2, pp. 707–750, 2016. doi:10.1109/TNS.2015.2485164

[3] H. Hähnel, A. Ates, and U. Ratzinger, "Update on the first 3D printed IH-type linac structure - proof-of-concept for additive manufacturing of Linac RF cavities", in *Proc. LINAC'22*, Liverpool, UK, Aug. 2022, pp. 170–173. doi:10.18429/JACoW-LINAC2022-MOPOGE11

[4] H. Hähnel *et al.*, "Additive manufacturing of an IH-type linac structure from stainless steel and pure copper", *Instruments*, vol. 7, no. 3, p. 22, 2023. doi:10.3390/instruments7030022

[5] H. Hähnel *et al.*, "RF conditioning of an IH-DTL cavity made using additive manufacturing", in *Proc. IPAC'24*, Geneva, Switzerland, May 2024, pp. 3495–3498. doi:10.18429/JACoW-IPAC2024-THPR10

[6] M. Mayerhofer *et al.*, "A 3D printed pure copper drift tube linac prototype", *Review of Scientific Instruments*, vol. 23, no. 2, p. 023304, 2022. doi:10.1063/5.0068494

[7] M. Mayerhofer *et al.*, "Improving fabrication and performance of additively manufactured RF cavities by employing co-printed support structures and their subsequent removal", *Instruments*, vol. 8, no. 1, p. 18, 2024. doi:10.3390/instruments8010018

[8] M. Mayerhofer *et al.*, "Additive manufacturing of side-coupled cavity linac structures from pure copper: A first concept", *Instruments*, vol. 7, no. 4, p. 56, 2023. doi:10.3390/instruments7040056

[9] M. Mayerhofer, J. Mitteneder, C. Wittig, I. Prestes, E. Jägle, and G. Dollinger, "First high quality DTL cavity additively manufactured from pure copper", in *Proc. IPAC'23*, Venice, Italy, May 2023, pp. 4967–4970. doi:10.18429/JACoW-IPAC2023-THPM035

[10] T. Torims *et al.*, "Evaluation of geometrical precision and surface roughness quality for the additively manufactured radio frequency quadrupole prototype", vol. 2420, no. 1, p. 012089, 2023. doi:10.1088/1742-6596/2420/1/012089

[11] T. Romano *et al.*, "Metal additive manufacturing for particle accelerator applications", *Physical Review Accelerators and Beams*, vol. 27, no. 5, p. 054801, 2024. doi.:10.1103/PhysRevAccelBeams.27.054801

[12] M. Mayerhofer *et al.*, "Red and green laser powder bed fusion of pure copper in combination with chemical post-processing for RF cavity fabrication", *Instruments*, vol. 8, no. 3, p. 39, 2024. doi:10.3390/instruments8030039

[13] B.T. McAllister *et al.*, "Characterization of cryogenic material properties of 3-D-printed superconducting niobium using a 3-D lumped element microwave cavity", *IEEE Transactions on Instrumentation and Measurement*, vol. 70, p. 1–7, 2020. doi:10.1109/TIM.2020.3031364